Journal of Molecular Graphics and Modelling 46 (2013) 132–139

Contents lists available at ScienceDirect

Journal of Molecular Graphics and Modelling

journal homepage: www.elsevier.com/locate/JMGM

Molecular dynamics simulations studies and free energy analysis on inhibitors of MDM2–p53 interaction

Rui-Juan Niu, Qing-Chuan Zheng*, Ji-Long Zhang, Hong-Xing Zhang*

State Key Laboratory of Theoretical and Computational Chemistry, Institute of Theoretical Chemistry, Jilin University, Changchun 130023, China

ARTICLE INFO

Article history:
Received 4 May 2013
Received in revised form
12 September 2013
Accepted 10 October 2013
Available online 24 October 2013

Keywords:
MD simulations
MM-GBSA
Binding free energy
MDM2–p53 interaction
Conformational mobility

ABSTRACT

The oncoprotein MDM2 (murine double minute 2) negatively regulates the activity and stability of tumor suppressor p53. Inactivation of the MDM2–p53 interaction by potent inhibitors offers new possibilities for anticancer therapy. Molecular dynamics (MD) simulations were performed on three inhibitors–MDM2 complexes to investigate the stability and structural transitions. Simulations show that the backbone of MDM2 maintains stable during the whole time. However, slightly structural changes of inhibitors and MDM2 are observed. Furthermore, the molecular mechanics generalized Born surface area (MM-GBSA) approach was introduced to analyze the interactions between inhibitors and MDM2. The results show that binding of inhibitor pDIQ to MDM2 is significantly stronger than that of pMI and pDI to MDM2. The side chains of residues have more contribution than backbone of residues in energy decomposition. The structure–affinity analyses show that L54, I61, M62, Y67, Q72, H73 and V93 produce important interaction energy with inhibitors. The residue W/Y22′ is also very important to the interaction between the inhibitors and MDM2. The three-dimensional structures at different times indicate that the mobility of Y100 influences on the binding of inhibitors to MDM2, and its change has important role in conformations of inhibitors and MDM2.

1. Introduction

In tumors, p53 protein is a potent inducer of cell cycle arrest, DNA repair, cellular senescence, innate immunity and apoptosis [1–3]. The E3 ubiquitin ligase MDM2 is one of the principal p53 modulators. It binds directly to the p53 transactivation domain and inhibits p53-dependent transcription [2,4]. Thus, reactivation of p53 by the inhibition of its binding to MDM2 is regarded as an effective and confirmed approach in cancer therapy [5]. Many reports have demonstrated the relevance between MDM2 inhibition and growth inhibition of cancer cells [4,6,7].

The side chains of hydrophobic residues F19′, W23′ and L26′ are responsible for the interaction of p53 with MDM2 [8–10]. The binding of p53 to MDM2 is directly disrupted by these residues and it may be an attractive pathway of targeted anticancer therapy [11–13]. Many drug candidates, such as small-molecule inhibitors, peptides, and peptide-analog are designed to target the interaction between p53 and MDM2. And the design novel potent inhibitors have become the current goal for cancer therapy development [14,15].

Recently, two peptide inhibitors pDI (LTFEHYWAQLTS) and pMI (TSFAEYWNLLSP) was identified using phage display [2,16–18]. Using pDI and pMI for comparison, a quadruple mutant peptide (pDIQ) was reported as the most potent inhibitor against MDM2 [19]. And the IC_{50} values determined by ELISA are pDIQ (8 nm), pMI (20 nm) and pDI (44 nm), respectively [19]. Three residues F19′, W23′ and L26′ of the inhibitors are critical residues for binding to MDM2. The dynamics, flexibility and conformational changes of three complexes have not been detailed discussed.

Molecular dynamics (MD) simulations are a powerful tool to complement experimental results with detailed dynamics behavior of biomolecules [20,21]. Binding free energy calculations and analysis have been proven to be powerful and valuable tools for understanding mechanisms of inhibitors to proteins [22]. MM-GBSA method has been proposed to be one of effective methods to calculate the binding free energies of inhibitors to proteins [23–25]. It has been successfully used to explain protein–protein and protein–inhibitor interactions [26–32]. In this work, molecular dynamics simulations combined with MM-GBSA method was applied to study the binding free energies of three inhibitors to MDM2. In addition, the energy decomposition analysis was carried out with the MM-GBSA approach. The detailed van der Waals, electrostatic, polar solvation, and nonpolar solvation energies between these inhibitors and individual MDM2 residues were calculated using per-residue-based decomposition method [33]. These results provide the difference in binding modes of the three inhibitors and

* Corresponding authors. Tel.: +86 431 88498966; fax: +86 431 88498966.
E-mail addresses: zhengqc@jlu.edu.cn (Q.-C. Zheng), zhanghx@mail.jlu.edu.cn (H.-X. Zhang).

1093-3263/$ – see front matter © 2013 Elsevier Inc. All rights reserved.
http://dx.doi.org/10.1016/j.jmgm.2013.10.005

reveal the main energy contribution of inhibitors binding to MDM2. In addition, the effects of the inhibitors and residue Y100 on the dynamics of MDM2 were analyzed. We suggest that these results can provide useful insights into the mechanisms of inhibition of the p53–MDM2 interaction.

2. Methods

2.1. System setups

The crystal structures of MDM2 complex with three peptide inhibitors (pDIQ, pMI and pDI) were obtained from the protein data bank (PDB) [34]. The PDB entries are 3JZS, 3EQS, and 3G03 [17–19]. These three structures were used for the starting model of MD simulations. All missing hydrogen atoms in MDM2 were added with the leap module in AMBER 11 package [35].

The ff99SB force field was applied to produce the parameters for the three models. An appropriate number of Cl^- counter ions were added to neutralize the charges of the systems. Finally, the whole system was solvated in an octahedral periodic box of TIP3P water molecules, and the distance between the edges of the water box and the closest atom of the solutes was at least 9.0 Å.

2.2. Molecular dynamics simulations

Energy minimizations and MD simulations were performed for each system using the SANDER module of AMBER 11 package. First, the water molecules and counter ions were minimized by positional restraints of 100 kcal/(mol Å^2) on the protein and inhibitor atoms to remove the bad contacts. Second, the entire system was minimized without any restraint. Each step was consisted of a 4000-step steepest descent and a 4000-step conjugate gradient minimization. After minimization, the system was gradually heated from 0 to 300 K in 200 ps with a position restraint of 10 kcal/(mol Å^2) in the C_α atoms of the complex. This followed by constant temperature equilibration at 300 K for another 200 ps. Finally, 50 ns MD simulations of each system at 1 atm and 300 K were carried out in an isothermal isobaric ensemble (NPT) with periodic boundary conditions. During the simulation, the SHAKE method was applied to constraint the covalent bonds involving hydrogen atoms [36,37]. An integration step of 2 fs was set for the MD simulations and the Particle Mesh Ewald (PME) method was used for calculating the long-range electrostatic interactions [38,39]. The cutoff distances for the long-range electrostatic and van de Waals energy interaction were set to 12 Å.

2.3. MM-GBSA calculation

For each complex, 1000 snapshots were extracted from the last 10 ns along the MD trajectory at an interval of 10 ps. The MM-GBSA method and nmod module, which implemented in Amber 11, were performed to compute the binding free energies of the three complex systems. In this method, the binding energy (ΔG) can be represented as:

$$\Delta G_{\text{bind}} = G_{\text{complex}} - G_{\text{protein}} - G_{\text{inhibitor}} \quad (1)$$

each free energy term in Eq. (1) is computed as a sum of gas phase molecular mechcanical energy (E_{gas}), the solvation free energy (E_{sol}), and the entropy term ($-T\Delta S$), using Eq. (2):

$$\Delta G_{\text{bind}} = E_{\text{gas}} + G_{\text{sol}} - T\Delta S \quad (2)$$

E_{gas} can be further divided into two parts:

$$E_{\text{gas}} = E_{\text{ele}} + E_{\text{vdW}} \quad (3)$$

where E_{ele} and E_{vdW} are described as the electrostatic interaction and van der Waals energy in the gas phase, respectively. The solvation free energy is expressed as:

$$G_{\text{sol}} = G_{\text{gb}} + G_{\text{nonp}} \quad (4)$$

where G_{gb} and G_{nonp} are the polar and non-polar contributions to solvation free energy. The polar component was computed using the GBSA program. The dielectric constants were set to 1 and 80 for the solute and surrounding solvent respectively in our calculations. The non-polar contribution was defined by the equation:

$$\Delta G_{\text{nonp}} = \gamma \text{SASA} + \beta \quad (5)$$

where SASA is the solvent accessible surface area estimated with a probe radius of 1.4 Å. γ and β are empirical constants and were set as 0.0072 kcal/(mol Å^2) and 0 kcal/mol for GB method. The conformational entropy change upon inhibitor binding ($-T\Delta S$), was obtained from the sum of the translational, rotational, and vibrational components, with the Nmode module of Amber 11.

2.4. Inhibitor–residues interaction decomposition

The interaction energies were further decomposed into contributions from protein and inhibitor residue pairs, which can only use the MM-GBSA method. The binding energy of each residue pair consists of three terms:

$$\Delta G_{\text{inhibiotr-residue}} = E_{\text{ele}} + E_{\text{vdW}} + G_{\text{gb}} + G_{\text{surf}} \quad (7)$$

where E_{ele} and E_{vdW} are described as non-bonded electrostatic interaction and van der Waals energy between the inhibitor and each MDM2 residue in the gas phase, respectively. And G_{gb} and G_{surf} are the polar and non-polar contributions for the inhibitor–residue interaction.

3. Results and discussion

3.1. Stability during MD simulations

To evaluate the reliable stability of the MD trajectories and the differences in the stabilities of MD simulations, the RMSD values of C_α atoms of MDM2 with respect to the starting structure over the 50 ns simulations are monitored. As shown in Fig. 1, the three complexes have reached the equilibrium and the RMSD values of 3JZS, 3EQS and 3G03 are ~1.20 Å after the 30 ns simulations, indicating good agreement with the X-ray crystal structures. And the deviations are under 0.12 Å in all three MD simulations. These results showed that the trajectories of MD simulations we used for post analyses of the three complexes are reliable.

To quantitatively measure the mean backbone mobility for each residue, the root mean square fluctuations (RMSF) values of MDM2 C_α relative the starting structure over the 50 ns simulations were calculated, as shown in Fig. 2. The results indicate that the mobility of the loops L2, L5 and the helixes $\alpha1'$, $\alpha2$, $\alpha2'$ domains are more obvious in the 3G03 structure than in 3JZS and 3EQS structures.

3.2. Binding free energies calculations

To further evaluate the difference in the binding modes of inhibitors to MDM2 and obtain detailed insights into the effect of each component contributed to the inhibitor–protein binding, the binding free energies of protein–inhibitor complexes are examined using MM-GBSA methods. The calculated results and experimental data are summarized in Table 1. The binding free energies of inhibitors to MDM2 are 3JZS (−21.03 kcal/mol), 3EQS (−14.62 kcal/mol) and 3G03 (−13.57 kcal/mol), respectively. These

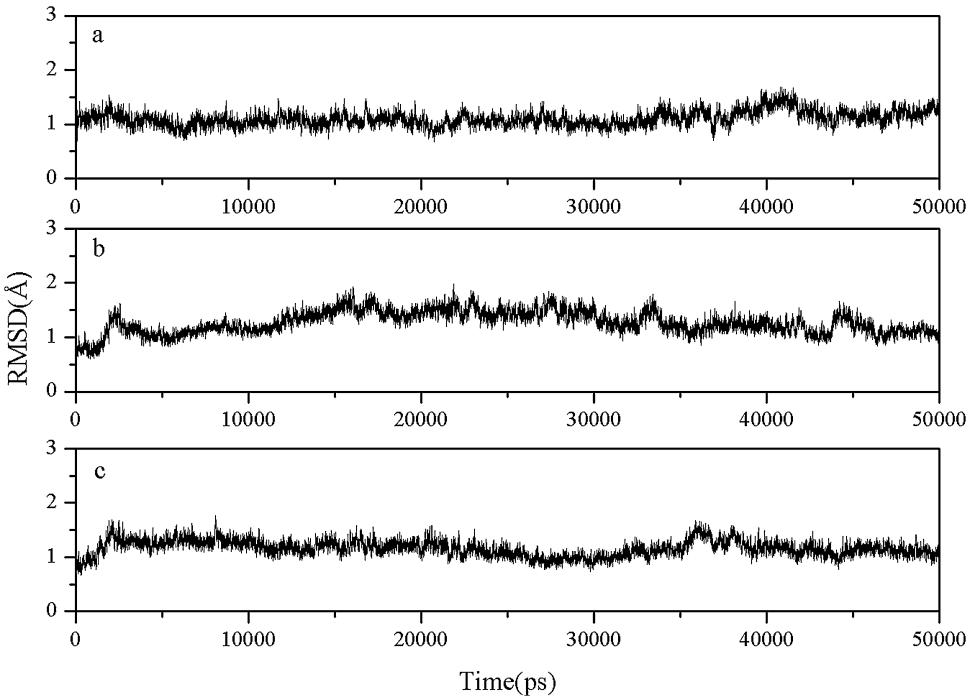

Fig. 1. The time dependence of RMSD values of backbone atoms in MD simulations for 3JZS (a), 3EQS (b) and 3G03 (c).

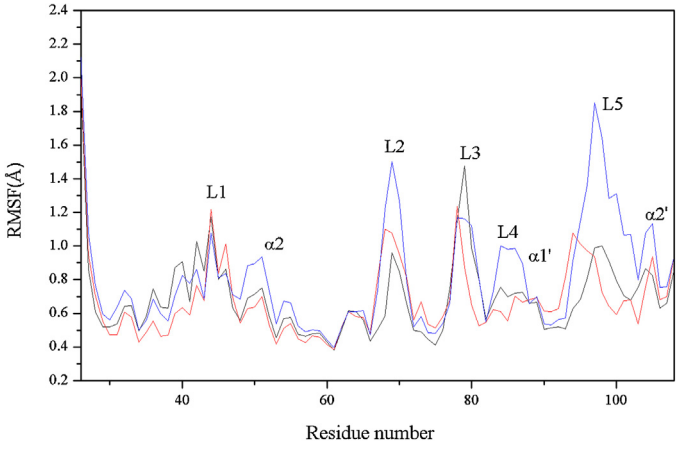

Fig. 2. The RMSF values of backbone atoms of MDM2 in the three complexes (3JZS: black, 3EQS: red and 3G03: blue) during the 50 ns simulations. (For interpretation of the references to color in this figure legend, the reader is referred to the web version of this article.)

predicted results are consistent with the experimental binding free energies.

As shown in Table 1, the electrostatic energies (E_{ele}) favor inhibitor binding and they have the largest values among the five components. But the favorable contributions of the electrostatic energies (E_{ele}) are completely screened by the strongest unfavorable polar solvation energies (G_{pol}). The major favorable contributors to the inhibitor binding are van der Waals energies (E_{vdW}). The non-polar solvation energies (G_{nonp}), which correspond to the burial of SASA upon binding, also provide important contribution to binding.

Table 2
The vdW energy contributions (kcal/mol) of critical residues at hydrophobic surface cleft of MDM2 to the binding.

Residue	3JZS	3EQS	3G03
L54	−2.74	−2.34	−2.56
L57	−1.23	−1.17	−1.12
G58	−1.53	−1.50	−1.46
I61	−1.71	−1.71	−1.68
M62	−1.70	−1.46	−1.71
Y67	−1.71	−1.93	−1.92
Q72	−3.72	−3.79	−3.62
H73	−2.25	−2.23	−1.67
V93	−3.27	−3.31	−3.14
K94	−1.94	−0.75	−1.90
H96	−2.51	−2.13	−2.03
I99	−0.99	−1.22	−1.11
Y100	−0.95	−0.61	−1.07

Table 1
Free energy analysis (kcal/mol) for the binding of inhibitors to MDM2 calculated by MM-GBSA method.[a]

Component[b]	3JZS	3EQS	3G03
E_{ele}	−370.88 (47.15/1.49)	−230.57 (26.41/0.83)	−206.03 (30.42/0.96)
E_{vdW}	−68.84 (4.98/0.16)	−59.34 (3.66/0.11)	−62.76 (3.83/0.12)
G_{pol}	395.94 (46.13/1.46)	253.44 (25.38/0.80)	232.72 (28.25/0.89)
G_{nonp}	−8.77 (0.62/0.02)	−8.13 (0.42/0.01)	−7.91 (0.42/0.01)
$-T\Delta S$	31.52 (0.00)	29.98 (0.00)	30.41 (0.00)
ΔG_{bind}	−21.03 (5.85)	−14.62 (3.81)	−13.57 (4.62)
ΔG_{exp}	−11.06	−10.51	−10.04

[a] All values are given in kcal/mol. Numbers in the parentheses present the standard deviations and standard errors.
[b] Component: E_{ele}, electrostatic energy; E_{vdW}, van der Waals energy; G_{nonp}, non-polar solvation energy; G_{pol}, polar solvation energy; $-T\Delta S$, total entropy contribution; $\Delta G_{bind} = E_{vdW} + E_{ele} + G_{nonp} + G_{pol} - T\Delta S$.

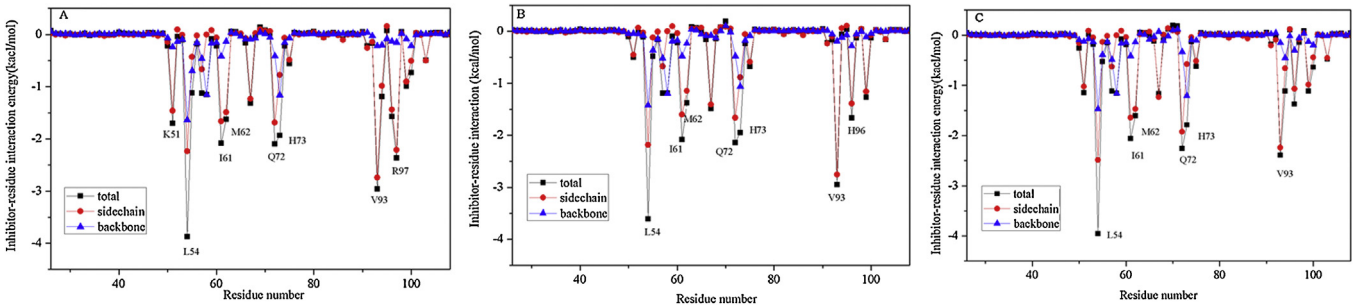

Fig. 3. Decomposition of the binding free energies on a per-residue basis for 3JZS (A), 3EQS (B), 3G03 (C) complexes based on MM-GBSA method.

3.3. Inhibitor–residue interaction decomposition

In order to obtain a more-detailed insight into the binding modes of three inhibitors to MDM2, the ΔG_{bind} is further decomposed into individual residue contributions using MM-GBSA method for the three complexes. Fig. 3 gives the interactions of the inhibitors with individual residues. The inhibitor–residue interaction has been performed to complement the previous energy analysis. L54, I61, Q72, H73 and V93 are the five common residues locate in the hot spot of the surface between the inhibitors and MDM2 [27]. It is also shown that the side chains of residues have more contribution than backbone of residues. Table 2 lists the van der Waals energy contributions of these critical residues on the binding. It confirms that the major favorable contributors to the inhibitor binding are van der Waals energies. The results are very helpful in understanding the mechanistic basis for the inhibitor–protein complex.

For the three complexes (3JZS, 3EQS and 3G03), the residue L54 produces the strongest interaction with the inhibitors. The atom NE1 of W23′ provides a hydrogen atom to form a hydrogen bond

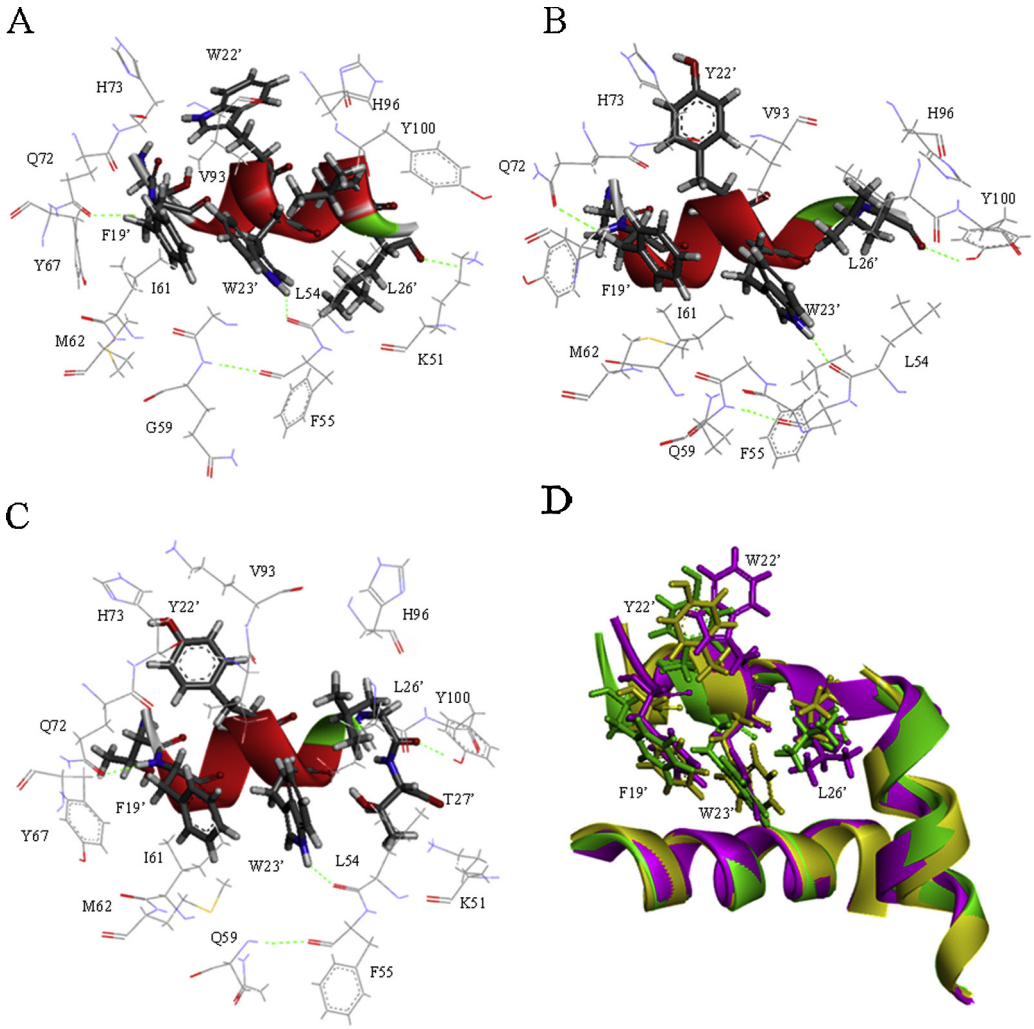

Fig. 4. The key residues which produce some favorable interactions with three inhibitors (A, B and C) and the superimpositions of the backbone atoms of the last structure (D). (A) 3JZS complex, (B) 3EQS complex, (C) 3G03 complex, (D) 3JZS: purple, 3EQS: green and 3G03: yellow. The green dashed line represents a hydrogen bond. (For interpretation of the references to color in this figure legend, the reader is referred to the web version of this article.)

Table 3
Hydrogen bonds between the inhibitors and MDM2.

Donor	Acceptor	Distance (Å)			Occupancy (%)		
		3JZS	3EQS	3G03	3JZS	3EQS	3G03
Q59-N	F55-O	3.00	2.98	2.95	98.14	98.99	99.15
L54-O	W23′-NE1-HE1	2.91	3.00	2.92	99.36	88.35	98.24
Q72-OE1	F19′-N-H	3.02	2.95	2.95	70.86	89.80	97.50

Table 4
Decomposition of the binding free energies on a per-residue basis for three inhibitors based on MM-GBSA method.[a]

Residue	3JZS			3EQS			3G03		
	E_t[2]	E_s	E_b	E_t	E_s	E_b	E_t	E_s	E_b
F19′	−7.33	−5.52	−1.81	−7.62	−5.72	−1.90	−7.49	−5.43	−2.06
W/Y22′	−4.55	−4.41	−0.14	−3.16	−2.85	−0.31	−4.20	−3.82	−0.38
W23′	−6.11	−5.44	−0.67	−5.82	−5.47	−0.35	−5.42	−5.18	−0.24
L26′	−4.16	−3.94	−0.22	−5.69	−4.45	−1.24	−4.43	−3.90	−0.53

[a] All values are given in kcal/mol.

with the atom O of L54. The occupancies of the hydrogen bond in 3JZS, 3EQS and 3G03 complexes are 99.36%, 88.35% and 98.24%, respectively. The information of the dynamics analysis of hydrogen bonds based on MD simulation is list in Table 3. Additionally, there is a direct Q59 N-F55 O hydrogen bond and the occupancies are 98.14% (3JZS), 98.99% (3EQS) and 99.15% (3G03). The results suggest that these hydrogen bonds are very stable during MD simulation. The direct hydrogen bond is different with most MDM2 structures and is likely entropically stabilizes the complex [4]. The atom N in the backbone of F19′ provides a hydrogen atom to construct a hydrogen bond with atom OE1 of Q72. The occupancies of the hydrogen bond are 70.86% (3JZS), 89.90% (3EQS) and 97.50% (3G03). Fig. 4 depicts the relative positions of the inhibitors and correlated residues in the binding complex using the last structure taken from the MD trajectories. These hydrogen bonds are also shown in green dashed lines in Fig. 4. These results indicate that the interactions undoubtedly contribute to the tight binding of the inhibitors.

According to Fig. 3, the residue K51 produces the interaction of −1.70 kcal/mol with pDIQ in the 3JZS complex. Besides the hydrogen bonds shown in Table 3, there is another hydrogen bond between the K51 NZ and L27′ O in 3JZS complex and the occupancy of this hydrogen bond is 49.05%. As shown in Fig. 4, the phenol of residue Y67 and the phenyl of F19′ generate an almost paralleled π–π interaction. As shown in Fig. 3, V93 contributes larger interaction energies to pDIQ, pMI and pDI. It is found that the alkyl of residue V93 not only generate the CH–π with the phenyl of F19′ and the indole of W23′, but also the CH–CH interaction with the L26′. These residues produce important interaction energies with inhibitors. And they are important residues that match the hydrophobic pockets to which F19′, W23′ and L26′ bind. For the 3EQS and 3G03 complexes, pMI and pDI lose the hydrogen bond between L27′ and K51 and the hydrophobic interactions of pMI and pDI with the residues in the active pockets are lower than in 3JZS complex. There is another hydrogen bond between the L26′ and Y100. But the occupancies of the hydrogen bond are lower.

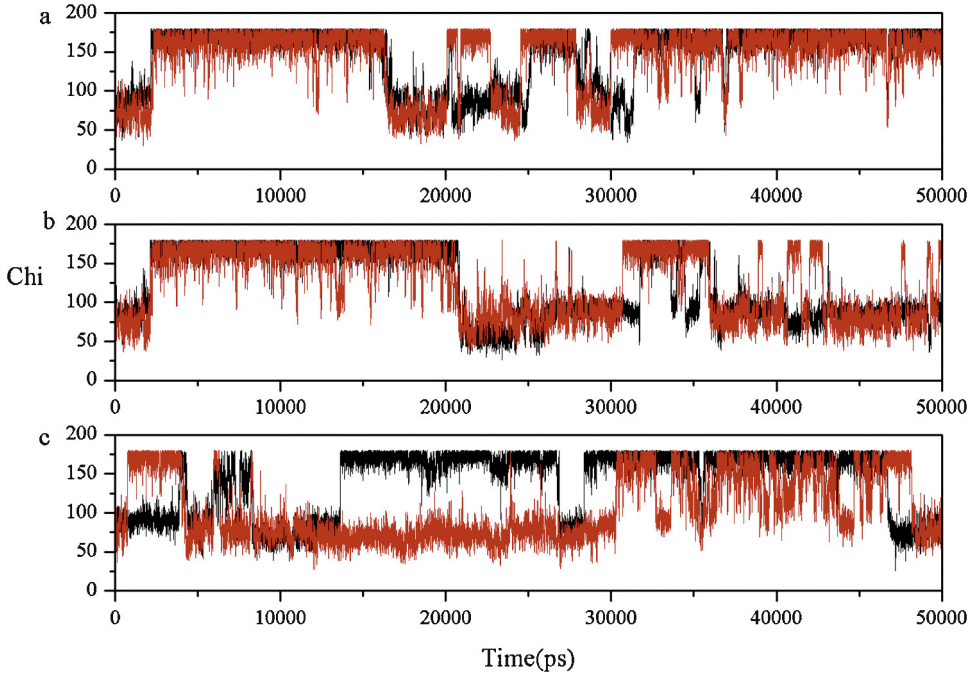

Fig. 5. The Chi1 (χ1, in degree) dihedral angle of the side chain of Y100 (black) and Y104 (red) as a function of time (a: 3JZS, b: 3EQS and c: 3G03). (For interpretation of the references to color in this figure legend, the reader is referred to the web version of this article.)

Fig. 6. Snapshots of the average structures of three complexes at the corresponding time during the simulations and the superimposition of these average structures (A: 3JZS, B: 3EQS and C: 3G03; a: 9–11 ns, b: 18–19 ns, c: 40–42 ns, d: 49–50 ns, e: superimposition of a, b, c, and d). The MDM2 and inhibitors are shown in cartoon mode, and the residues Y100 and Y104 are displayed in line and F19′, W23′ and L26′ are shown in stick.

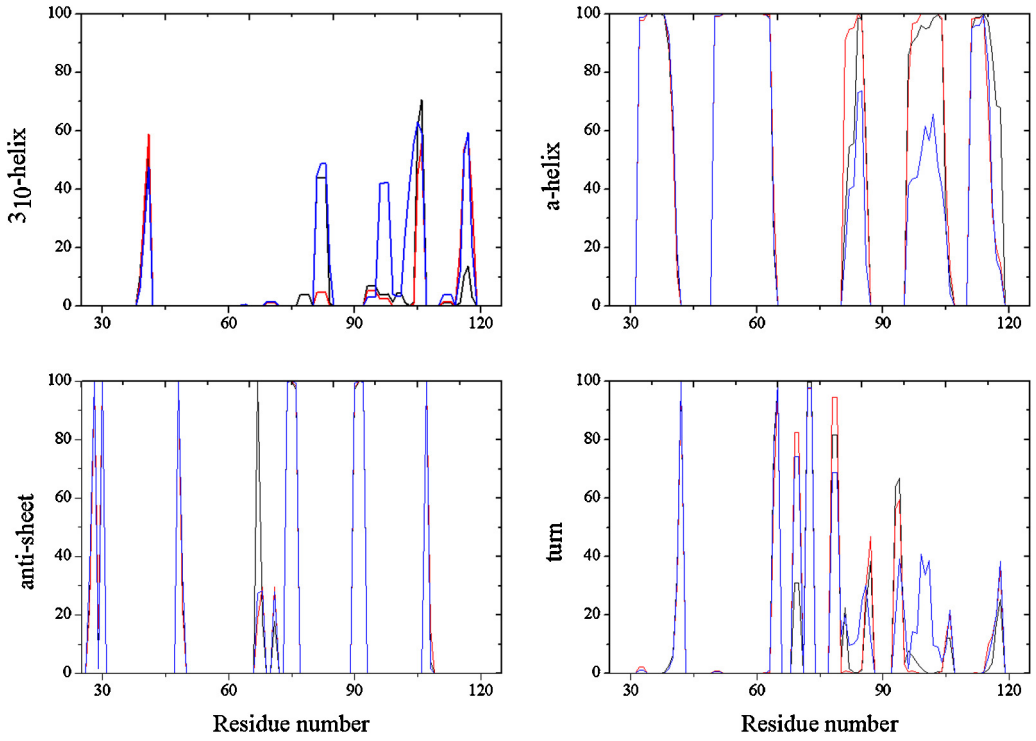

Fig. 7. The secondary structure content of the MD simulation is calculated for each system. Black: 3JZS complex; red: 3EQS complex; blue: 3G03 complex. (For interpretation of the references to color in this figure legend, the reader is referred to the web version of this article.)

Fig. 4D gives the superimpositions of the backbone atoms of the three complexes, and some residues are also shown in stick and line. The individual residues of the inhibitors are also analyzed to illustrate the specific features in the inhibitors. The total, side chain and backbone energy decomposition of the four residues is shown in Table 4. We find that the most obviously difference is the residue W22′/Y22′. And the side chains provide more energy contribution than the backbone atoms. Except the three critical residues, W22′/Y22′ is also important in the inhibitor binding to MDM2. The phenomenon is that the side chain of W22′ is indole while the Y22′ is phenol. As seen from Fig. 4, W22′ provides more CH–π interaction contacts with MDM2 than Y22′. These results indicate that the interactions undoubtedly contribute to the tight binding of the inhibitors.

Based on the above analysis, the three inhibitors bind to MDM2 in similar binding mode. But they produce different interaction contacts with MDM2. The side chains have more contribution than backbone atoms. The residue W/Y22′ is also very important to the interaction except the three critical residues F19′, W23′ and L26′.

3.4. The mobility of Y100 and the conformation change of inhibitors and MDM2

In order to evaluation the mobility role of Y100 on the conformation change of MDM2, the Chi1 ($\chi 1$) dihedral angle of the side chain of Y100 and Y104 are shown in Fig. 5. The mobility of Y104 is correlated strongly with that of Y100 in 3JZS and 3EQS complexes, which is not found in 3G03 complex. And the magnitude of fluctuation of side chain of Y104 is larger after 30 ns in 3G03 complex. Several three-dimensional structures at different times along with the changing processes of the studied MDM2 and inhibitor complexes are shown in Fig. 6. The conformations of side chains of the critical residues F19′ and W23′ do not obviously change during the MD simulations for different inhibitors. However, the residue conformations of L26′ is different at different time. Fig. 7 shows the secondary structure content of the MD simulation of the three systems. Comparing with the 3JZS and 3EQS complexes, the mobility of the α2′ and α1′ helix and of 3G03 are more obvious during the MD simulation time. The nature basically agrees with the previous RMSF analyses. It is clear to observe that residues at 81–83, 96–98, and 102–104 domains are tend to be 3_{10} helix, while the secondary content of residues at 99–101 are about tend to be coil in 3G03 structure. This phenomenon can be also seen in Fig. 6C. It might the reason that the mobility of Y104 is nor correlated with that of Y100.

The variability conformation mobility of Y100 might influence on the secondary structures, which would lead to structure changes of MDM2 and unstable MDM2–pDI binding. The results are in accordance with several MD simulations of the conformational mobility of Y100 [40,41].

4. Conclusions

Based on the fifty nanoseconds of MD simulations and the analysis of dynamics properties, the binding modes, affinities and structural transitions are investigated on three potent peptides in disrupting MDM2–p53 binding. Simulations show that three complexes maintain stable, however, slightly structural changes of inhibitors and MDM2 were observed. The MM-GBSA binding free energy calculations show that binding of inhibitor pDIQ to MDM2 is significantly stronger than that of pMI and pDI to MDM2. And the van der Waals energies, non-polar solvation energies and the entropy changes to the free energies provide important contribution to binding. The side chains of residues have more contribution than backbone of residues in energy decomposition. The residue W/Y22′ is also very important to the interaction between the inhibitors and MDM2. Especially, the mobility of Y100 influences on the binding of inhibitors to MDM2, and its change has important role in complex conformations of inhibitors and MDM2.

Acknowledgment

This work is supported by Natural Science Foundation of China (Grant Nos. 21273095, 20903045 and 21203072).

References

[1] A. Takaoka, S. Hayakawa, H. Yanai, D. Stoiber, H. Negishi, H. Kikuchi, S. Sasaki, K. Imai, T. Shibue, K. Honda, T. Taniguchi, Integration of interferon-alpha/beta signalling to p53 responses in tumour suppression and antiviral defence, Nature 424 (2003) 516–523.
[2] A.J. Levine, p53, the cellular gatekeeper for growth and division, Cell 88 (1997) 323–331.
[3] Y. Rew, D. Sun, F. Gonzalez-Lopez De Turiso, M.D. Bartberger, H.P. Beck, J. Canon, A. Chen, D. Chow, J. Deignan, B.M. Fox, D. Gustin, X. Huang, M. Jiang, X. Jiao, L. Jin, et al., Structure-based design of novel inhibitors of the MDM2–p53 interaction, J. Med. Chem. 55 (2012) 4936–4954.
[4] S. Baek, P.S. Kutchukian, G.L. Verdine, R. Huber, T.A. Holak, K.W. Lee, G.M. Popowicz, Structure of the stapled p53 peptide bound to Mdm2, J. Am. Chem. Soc. 134 (2012) 103–106.
[5] Z. Zhang, M. Li, H. Wang, S. Agrawal, R. Zhang, Antisense therapy targeting MDM2 oncogene in prostate cancer: effects on proliferation, apoptosis, multiple gene expression, and chemotherapy, Proc. Natl. Acad. Sci. U. S. A. 100 (2003) 11636–11641.
[6] M. Miyazaki, H. Kawato, H. Naito, M. Ikeda, M. Miyazaki, M. Kitagawa, T. Seki, S. Fukutake, M. Aonuma, T. Soga, Discovery of novel dihydroimidazothiazole derivatives as p53–MDM2 protein–protein interaction inhibitors: synthesis, biological evaluation and structure–activity relationships, Bioorg. Med. Chem. Lett. 22 (2012) 6338–6342.
[7] P. Chène, Inhibiting the p53–MDM2 interaction: an important target for cancer therapy, Nat. Rev. Cancer 3 (2003) 102–109.
[8] J.K. Muurray, S.H. Gellman, Targeting protein–protein interactions: lessons from p53/MDM2, Biopolymers 88 (2007) 657–686.
[9] P. Furet, P. Chène, A. De Pover, T.S. Valat, J.H. Lisztwan, J. Kallen, K. Masuya, The central valine concept provides an entry in a new class of non peptide inhibitors of p53–MDM2 interaction, Bioorg. Med. Chem. Lett. 22 (2012) 3498–3502.
[10] J. Mittal, T.H. Yoo, G. Georqiou, T.M. Truskett, Structural ensemble of an intrinsically disordered polypeptide, J. Phys. Chem. B. 117 (2013) 118–124.
[11] S. Shangary, S.M. Wang, Targeting the MDM2–p53 interaction for cancer therapy, Clin. Cancer Res. 14 (2008) 5318–5324.
[12] A.C. Joerger, A.R. Fersht, Structural biology of the tumor suppressor p53, Annu. Rev. Biochem. 77 (2008) 557–582.
[13] K.H. Vousden, D.P. Lane, p53 in health and disease, Nat. Rev. Mol. Cell Biol. 8 (2007) 275–283.
[14] M.R. Arkin, J.A. Wells, Small-molecule inhibitors of protein–protein interactions: progressing towards the dream, Nat. Rev. Drug Discovery 3 (2004) 301–317.
[15] S. Shangary, S.M. Wang, Small-molecule inhibitors of the MDM2–p53 protein–protein interaction to reactivate p53 function: a novel approach for cancer therapy, Annu. Rev. Pharmacol. Toxicol. 49 (2009) 223–241.
[16] B. Hu, D.M. Gilkes, J. Chen, Efficient p53 activation and apoptosis by simultaneous disruption of binding to MDM2 and MDMX, Cancer Res. 67 (2007) 8810–8817.
[17] A. Czarna, G.M. Popowicz, A. Pecak, S. Wolf, G. Dubin, T.A. Holak, High affinity interaction of the p53 peptide-analogue with human Mdm2 and Mdmx, Cell Cycle 8 (2009) 1176–1184.
[18] M. Pazgier, M. Liu, G.Z. Zou, W.R. Yuan, C.Q. Li, C. Li, J. Li, J. Monbo, D. Zella, S.G. Tarasov, W.Y. Lu, Structural basis of high-affinity peptide inhibition of p53 interactions with MDM2 and MDMX, Proc. Natl. Acad. Sci. 106 (2009) 4665–4670.
[19] J. Phan, Z.Y. Li, A. Kasprzak, B.Z. Li, S. Sebti, W. Guida, E. Schönbrunn, J.D. Chen, Structure-based design of high affinity peptide inhibiting the interaction of p53 with MDM2 and MDMX, J. Biol. Chem. 285 (2010) 2174–2183.
[20] W.F. van Gunsteren, H.J. Berendsen, Computer simulation of molecular dynamics: methodology, applications, and perspectives in chemistry, Angew. Chem. Int. Ed. 29 (1990) 992–1023.
[21] B.O. Brandsdal, F. Osterberg, M. Almlöf, I. Feierberg, V.B. Luzhkov, J. Aqvist, Free energy calculations and ligand binding, Adv. Protein Chem. 66 (2003) 123–158.
[22] M. Karplus, J.A. McCammon, Molecular dynamics simulations of biomolecules, Nat. Struct. Biol. 9 (2002) 646–652.
[23] J.M. Swanson, R.H. Henchman, J.A. McCammon, Revisiting free energy calculations: a theoretical connection to MM/PBSA and direct calculation of the association free energy, Biophys. J. 86 (2004) 67–74.
[24] J. Wang, P. Morin, P.A. Kollman, Use of MM-PBSA in reproducing the binding free energies to HIV-1 RT of TIBO derivatives and predicting the binging mode to HIV-1 RT of efavirenz by docking and MM-PBSA, J. Am. Chem. Soc. 123 (2001) 5221–5230.
[25] W. Wang, W.A. Lim, A. Jakalian, J. Wang, R. Luo, C.I. Bayly, P.A. Kollman, An analysis of the interactions between the Sem-5 SH3 domain and its ligands

using molecular dynamics, free energy calculations, and sequence analysis, J. Am. Chem. Soc. 123 (2001) 3986–3994.
[26] Y. Xu, R. Wang, A computational analysis of the binding affinities of FKBP12 inhibitors using the MM PB/SA method, Proteins 50 (2006) 1058–1068.
[27] L. Chen, J.L. Zhang, L.Y. Yu, Q.C. Zheng, W.T. Chu, Q. Xue, H.X. Zhang, C.C. Sun, Influence of hyperthermophilic protein Cren7 on the stability and conformation of DNA: insights from molecular dynamics simulation and free energy analysis, J. Phys. Chem. B. 116 (2012) 12415–12425.
[28] J.Z. Chen, J.N. Wang, B.S. Xu, W.L. Zhu, G.H. Li, Insight into mechanism of small molecule inhibitors of the MDM2–p53 interaction: molecular dynamics simulation and free energy analysis, J. Mol. Graph. Model. 30 (2011) 46–53.
[29] G. Hu, D. Wang, X. Liu, Q. Zhang, A computational analysis of the binding model of MDM2 with inhibitors, J. Comput. Aided Mol. Des. 24 (2010) 687–697.
[30] H. Zhong, H.A. Carlson, Computational studies and peptidomimetic design for the human p53–MDM2 complex, Proteins 58 (2005) 222–234.
[31] T. Hou, J. Wang, Y. Li, W. Wang, Assessing the performance of the MM/PBSA and MM/GBSA methods. 1. The accuracy of binding free energy calculations based on molecular dynamics simulations, J. Chem. Inf. Model. 51 (2011) 69–82.
[32] J. Guo, X. Wang, H. Sun, H. Liu, Y. Shen, X. Yao, The evolution of HLA-B*3501 binding affinity to variable immunodominant NP(418-426) peptides from 1918 to 2009 pandemic influenza A virus: a molecular dynamics simulation and free energy calculation study, Chem. Biol. Drug Des. 79 (2012) 1025–1032.
[33] H. Gohlke, C. Kiel, D.A. Case, Insights into protein–protein binding by binding free energy calculation and free energy decomposition for the Ras–Raf and Ras–RalGDS complexes, J. Mol. Biol. 330 (2003) 891–913.
[34] http://www.rcsb.org/pdb/home/home.do
[35] D.A. Case, T.A. Darden, T.E. Cheatham III, C.L. Simmerling, J. Wang, R.E. Duke, R. Luo, R.C. Walker, W. Zhang, K.M. Merz, B. Roberts, B. Wang, S. Hayik, A. Roitberg, G. Seabra, I. Kolossváry, K.F. Wong, F. Paesani, J. Vanicek, J. Liu, X. Wu, S.R. Brozell, T. Steinbrecher, H. Gohlke, Q. Cai, X. Ye, J. Wang, M.-J. Hsieh, G. Cui, D.R. Roe, D.H. Mathews, M.G. Seetin, C. Sagui, V. Babin, T. Luchko, S. Gusarov, A. Kovalenko, P.A. Kollman, AMBER 11, University of California, San Francisco, 2010.
[36] J.P. Ryckaert, G. Ciccotti, H.J.C. Berendsen, Numerical integration of the cartesian equations of motion of a system with constraints: molecular dynamics of *n*-alkanes, J. Comp. Phys. 23 (1977) 327–341.
[37] T.G. Coleman, H.C. Mesick, R.L. Darby, Numerical integration: a method for improving solution stability in models of the circulation, Ann. Biomed. Eng. 5 (1977) 322–328.
[38] T. Darden, D. York, L. Pedersen, Particle mesh Ewald: an *N*-log(*N*) method for Ewald sums in large systems, J. Chem. Phys. 98 (1993) 10089–10092.
[39] U. Essmann, L. Perera, M.L. Berkowitz, T. Darden, H. Lee, L.G. Pedersen, A smooth particle mesh Ewald method, J. Chem. Phys. 103 (1995) 8577–8593.
[40] S. Dastidar, D. Lane, C. Verma, Modulation of p53 binding to MDM2: computational studies reveal important roles of Tyr100, BMC Bioinform. 10 (15) (2009) S6.
[41] S. Dastidar, D. Lane, C. Verma, Multiple peptide conformations give rise to similar binding affinities: molecular simulations of p53–MDM2, J. Am. Chem. Soc. 130 (2008) 13514–13515.